Available online at www.sciencedirect.com
ScienceDirect
Nuclear Instruments and Methods in Physics Research A 585 (2008) 69–75
NUCLEAR INSTRUMENTS & METHODS IN PHYSICS RESEARCH Section A
www.elsevier.com/locate/nima

Rotating dual-wire beam profile monitor optimized for use in merged-beams experiments

D.G. Seely[a,*], H. Bruhns[b], D.W. Savin[b], T.J. Kvale[c], E. Galutschek[d], H. Aliabadi[d], C.C. Havener[d]

[a]*Department of Physics, Albion College, Albion, MI 49224-1831, USA*
[b]*Columbia Astrophysics Laboratory, Columbia University, New York, NY 10027-6606, USA*
[c]*Department of Physics and Astronomy, The University of Toledo, Toledo, OH 43606-3390, USA*
[d]*Physics Division, Oak Ridge National Laboratory, Oak Ridge, TN 37831-6372, USA*

Received 21 July 2007; received in revised form 21 October 2007; accepted 24 October 2007
Available online 4 November 2007

Abstract

A rotating dual-wire beam profile monitor based upon a National Electrostatics Corporation Model BPM80 beam profile monitor is described. The device can measure beam profiles in two perpendicular directions (horizontal and vertical) in each of two pseudoplanes that are situated along the beam axis and are separated by a distance of 5.4 cm. The output signal from the device is analyzed in real time to yield horizontal and vertical beam profiles and to calculate the divergence of a particle beam that traverses the device. This set-up is well-suited for merged-beams experiments where one beam is tuned to saved profiles from a second beam in order to minimize the merge angle and beam divergences while maximizing the beam–beam overlaps.

PACS: 07.77.Hj; 07.77.Gx; 07.77.Ka

Keywords: Beam profile monitor; Beam scanner; Rotating wire; Merged beams; Overlap

1. Introduction

In experiments that employ a merged-beams technique [1] the determination of an absolute cross section requires the measurement of the overlap of the two beams in the merge region. This is accomplished by integrating the product of the current densities, $j_1(x,y,z)$ and $j_2(x,y,z)$, over the merge region. The normalized overlap integral is defined as

$$\Omega = \frac{\int\int\int_V j_1(x,y,z)\, j_2(x,y,z)\,\mathrm{d}x\,\mathrm{d}y\,\mathrm{d}z}{\int\int\int_V j_1(x,y,z)\,\mathrm{d}x\,\mathrm{d}y\,\mathrm{d}z \int\int\int_V j_2(x,y,z)\,\mathrm{d}x\,\mathrm{d}y\,\mathrm{d}z}. \quad (1)$$

Here V specifies the volume of the interaction region. To make a measurement of Ω, it is thus necessary to evaluate the product $j_1(x,y,z)\, j_2(x,y,z)$ in the interaction region. This is generally problematic because of difficulties in sampling each beam at all points in the interaction volume. A common alternative approach is to define the axis of the merged beams as the z-axis and to measure two-dimensional current densities, $j_1(x,y)$ and $j_2(x,y)$, in planes perpendicular to this axis at a number of fixed positions in z. Typically, normalized beam overlap functions of the form

$$\Omega(z) = \frac{\int\int j_1(x,y)\, j_2(x,y)\,\mathrm{d}x\,\mathrm{d}y}{\int\int j_1(x,y)\,\mathrm{d}x\,\mathrm{d}y \int\int j_2(x,y)\,\mathrm{d}x\,\mathrm{d}y} \quad (2)$$

are evaluated at a number of fixed locations along the merged path [2,3]. It is thus desirable to have a device that can measure $j_1(x,y)$ and $j_2(x,y)$ and compute $\Omega(z)$. The goal in a merged beams experiment is to maximize $\Omega(z)$, and thus the degree to which the two beams overlap in space. It is highly desirable to do this in real time and in a minimally invasive manner, particularly when tuning the beams.

*Corresponding author. Tel.: +1 517 629 0361; fax: +1 517 629 0264.
E-mail address: dseely@albion.edu (D.G. Seely).

0168-9002/$ - see front matter © 2007 Elsevier B.V. All rights reserved.
doi:10.1016/j.nima.2007.10.041

The determination of the interaction energy requires the measurement of the merge angle θ between the beams, which also can be determined from the two-dimensional current density measurements. For two reactant beams with masses m_1 and m_2 and energies E_1 and E_2, the interaction energy in the center of mass reference frame is given by

$$E_{cm} = \frac{E_1}{m_1} + \frac{E_2}{m_2} - 2\sqrt{\frac{E_1 E_2}{m_1 m_2}}\cos\theta. \quad (3)$$

It is evident that θ must be made very small to achieve the lowest collision energies. At the lowest energies the beam divergence can be the major contribution to the collision energy uncertainty [1].

Various devices have been constructed to measure two-dimensional [3–8] or three-dimensional [9] beam profiles in merged-beam experiments. In many cases, particle fluxes transmitted across an aperture or apertures of known dimension are measured as the aperture is scanned across the beam. An exception is a video technique in which beams are directly imaged on a microchannel plate [8]. Scanning transmission devices, however, typically require acquisition times that exceed 1 min [3–6] for beam fluxes that correspond to current densities on the order of $1\,\mu A/mm^2$ because of the need to integrate in time the much smaller beam currents transmitted across the aperture to obtain good statistical significance. Video methods are faster, but the performance degrades in time due to beam damage [8] and the beam is destroyed by the profile measurement.

2. Dual-wire beam-profile monitor

An alternative method to measure beam profiles is to detect the secondary electrons that are produced when a thin conducting object, such as a moving wire, traverses the beam in a direction perpendicular to the beam axis. Two orthogonal beam scans are then required to characterize the beam. The advantages of this method are that it is non-destructive and can be done in real time. As the wire traverses the beam, the secondary electron current at any instant is proportional to the integrated beam current intercepted by the wire at the moment the secondary electrons were emitted by the wire. The measured beam profiles can be thus be represented by integral expressions of the form

$$I_i(x) = \varepsilon_i \int j_i(x,y)\,dy \quad (4)$$

$$I_i(y) = \varepsilon_i \int j_i(x,y)\,dx \quad (5)$$

where the index $i = 1, 2$ specifies the beam that is scanned. An efficiency factor, ε_i, accounts for the secondary emission coefficient of the wire and the efficiency of the electron collection system. With the assumption that the two-dimensional current densities $j_1(x,y)$ and $j_2(x,y)$ are separable in x and y, the normalized beam overlap function (Eq. (2)) can be written in terms of the measured quantities of Eqs. (4) and (5) as [6]

$$\Omega(z) = \frac{\int I_1(x) I_2(x)\,dx \int I_1(y) I_2(y)\,dy}{\int I_1(x)\,dx \int I_2(x)\,dx \int I_1(y)\,dy \int I_2(y)\,dy}. \quad (6)$$

For some two-dimensional beam density profiles, Eq. (6) may not be a good approximation of Eq. (2). One way to partially check the validity of using Eq. (6) is to acquire beam profiles in another coordinate system (x', y') that is tilted at an angle of 45° relative to the (x, y) coordinate system and to look for irregular effects in any or all of the one-dimensional profiles that suggest that the corresponding two-dimensional profiles have non-separable components (e.g., hollow beams, crescent shaped beams, etc.).

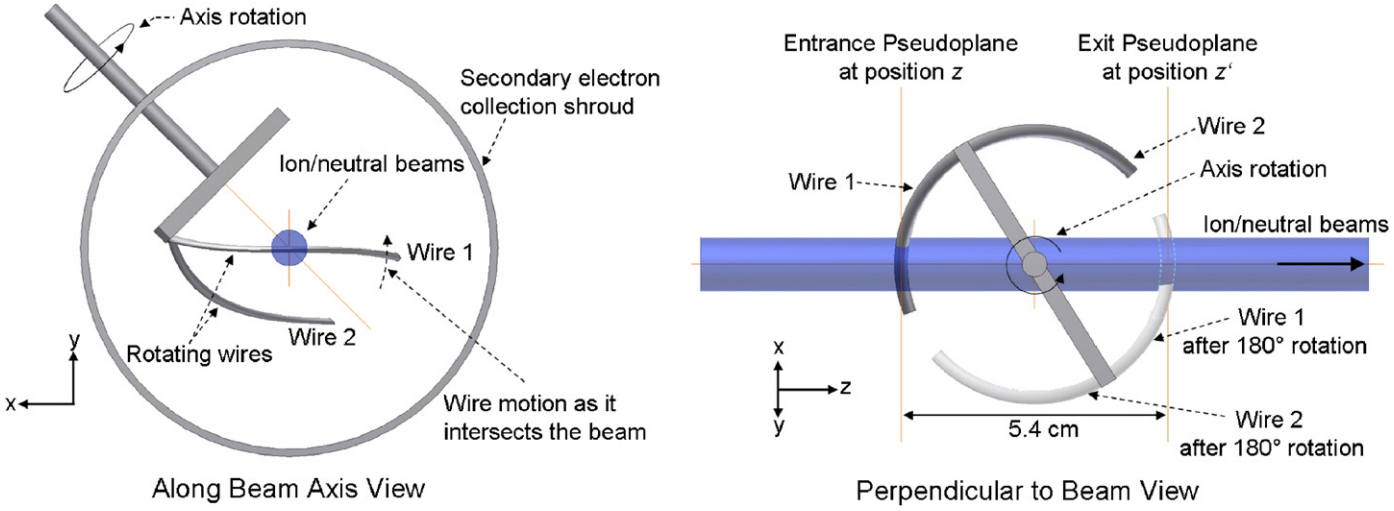

Fig. 1. Schematic drawings of the scanning wires (a) looking down the beam axis and (b) looking perpendicular to the beam at an instant when the scanner is generating the $I(y)$ profile. The viewpoint in (b) is from a point on the rotation axis of the scanner. In either view, Wire 1 is moving in the y direction, according to the coordinate system associated with the view. In (b) the positions of Wire 1 and Wire 2 are shown at the same instant as in (a) and after a 180° rotation.

Additionally, the profiles from the tilted system can be used to check for consistency in the calculation of Ω.

Rotating wire scanners [10–12] (devices which detect secondary electrons that are emitted when a conducting wire is rotated through a particle beam) have long been used to measure beam profiles in real time, but can be problematic because the x and y profiles measured by a traditional single-wire scanner are acquired at different locations along the beam axis z. Beam profiles can change significantly even over the few centimeters between the locations of the x and y profiles typical in commercial rotating wire scanners. Additionally, the electron collection efficiency of the scanning system may depend on z, which compounds the difficulties in comparing x and y profiles while tuning.

These problems can be addressed by adding a second wire to a rotating helical wire beam scanner [13]. In the investigation reported here, a prototype dual wire scanner was fabricated by the National Electrostatic Corporation (NEC) [14] which modified a commercially available NEC Model BPM80 single wire beam scanner. The BPM80 has a rotating wire that is formed into a $\frac{1}{8}$-turn (45°) helix and is mounted to a rotating support bar such that the axis of the helix is co-linear with the axis of rotation of the bar. A schematic view of the modified scanner is shown in Fig. 1. In the modified scanner, a second wire is mounted on the same end of the rotating support bar to which the first wire is attached. The second wire makes a 45° helix, like the first, but has opposite helicity. A small counterweight is attached to the other end of the support bar. Like its single wire counterpart, the motion of the scanner wires is approximately linear in the regions where the wires intersect the centerline of the scanner housing [15]. Hence, the surfaces traced by the wires in these regions are referred to as *pseudoplanes* by the manufacturer [15]. Also like its single wire counterpart, the dual wire scanner is mounted so that its axis of rotation is perpendicular to the beam axis and makes an angle of 45° relative to the desired x and y coordinate system. Usually the device is mounted so that the x and y directions are aligned with horizontal and vertical directions, respectively. During a single rotation of the wires, beam profiles along the x and y directions are produced in two pseudoplanes located at positions z and z', along the beam axis.

As noted above, beam profiles are generated by detecting secondary electrons that are produced when either of the rotating wires intersects the beam. The secondary electrons are collected by an isolated stainless steel cylinder with a

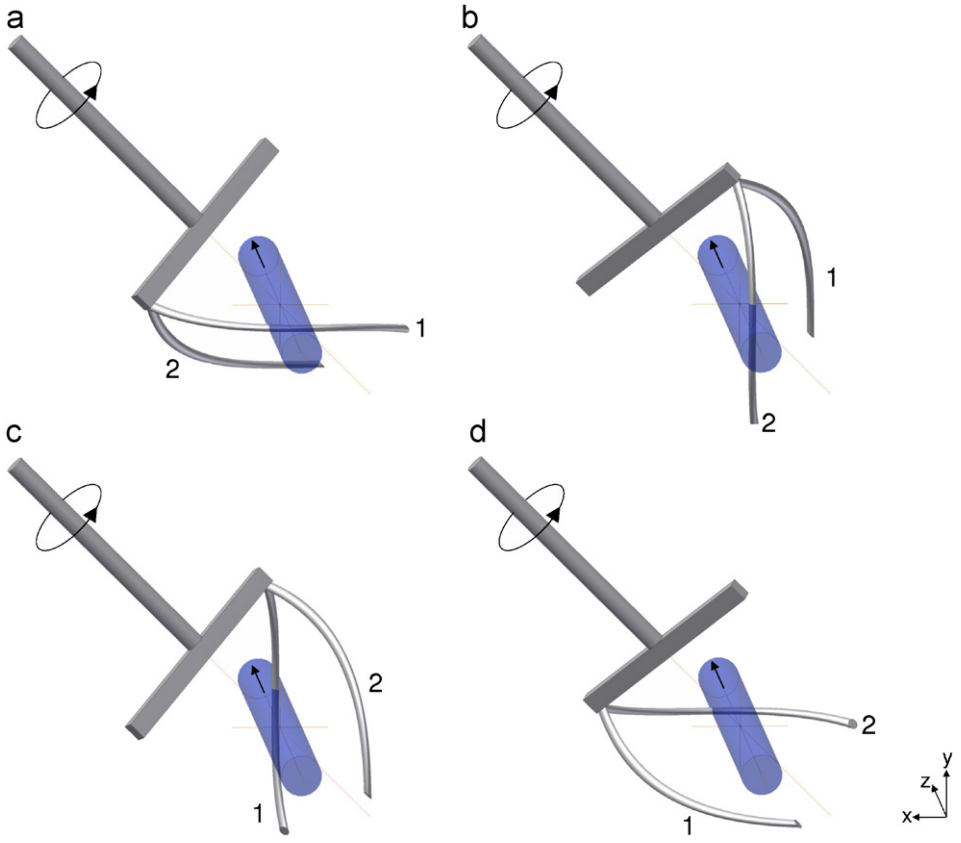

Fig. 2. Schematic drawings of the scanning wires looking from an oblique perspective that is nearly along the beam axis. The coordinate system is shown. The location of the wires are shown for the following four events: (a) horizontal wire in the first (upstream) pseudoplane crossing the axis in the vertical direction (− to + along y), (b) vertical wire in the first pseudoplane crossing the axis in the reverse horizontal direction (+ to − along x), (c) vertical wire in the second (downstream) pseudoplane crossing the axis in the horizontal direction (− to + along x) and (d) horizontal wire in the second pseudoplane crossing the axis in the reverse vertical direction (+ to − along y). The motion of the wires generates $I(y)$, $I(x)$, $I(x')$, and $I(y')$ profiles as labeled in Fig. 3.

diameter and length slightly smaller than the housing and which is mounted coaxial with the housing. A hole in the side of the cylinder permits the rotating shaft to protrude through the cylinder. The cylinder is electrically coupled to a sensitive current amplifier that is mounted just outside the housing [16]. The amplifier has an adjustable gain, settable in decades from 10^3 to 10^7 V/A and is sensitive to nanoampere currents. The output of the amplifier is connected to a waveform capture device, e.g. an oscilloscope.

The inner rotating shaft is magnetically coupled to an external rotor disk that is directly coupled to the shaft of the drive motor. The inner rotating assembly contains a disk with four magnetic pins spaced 90° apart that protrude radially outward from the periphery of the disk. The pins are located such that they will produce a signal pulse in an external magnetic sensor on each occasion that a rotating wire crosses the central axis. A fifth pin is located midway between two of the pins and is positioned closer to the detector so that it will produce a larger pulse in the magnetic sensor. A single rotation of the scanner will thus produce five pulses in the magnetic sensor. All these pulses are called "fiducial" pulses because they are uniquely correlated in time with the orientation of the scanner wires.

The orientations of the scanner wires at instants when each of the wires crosses the axis of the scanner housing are shown in Fig. 2. A sample fiducial waveform and a sample output waveform are shown in Fig. 3. In the waveform of fiducial pulses, the large pulse is used as a trigger pulse to signal the beginning of a cycle. The remaining four pulses locate the following four events: (1) horizontal wire in the first (upstream) pseudoplane crossing the scanner centerline axis in the vertical direction (from − to + along the along the y-axis shown) and producing a vertical beam profile, (2) vertical wire in the first pseudoplane crossing the scanner centerline axis in the horizontal direction (from + to − along the x-axis shown) and producing a "reverse" horizontal beam profile, (3) vertical wire in the second (downstream) pseudoplane crossing the scanner centerline axis in the horizontal direction (from − to + along the x-axis) and producing a horizontal beam profile, and (4) horizontal wire in the second pseudoplane crossing the scanner centerline axis in the vertical direction (from + to − along the y-axis) and producing a reverse vertical beam profile.

Fig. 2 is also helpful in visualizing how the different horizontal and vertical scans are generated by the motion of the wires. The output waveform shown in Fig. 3

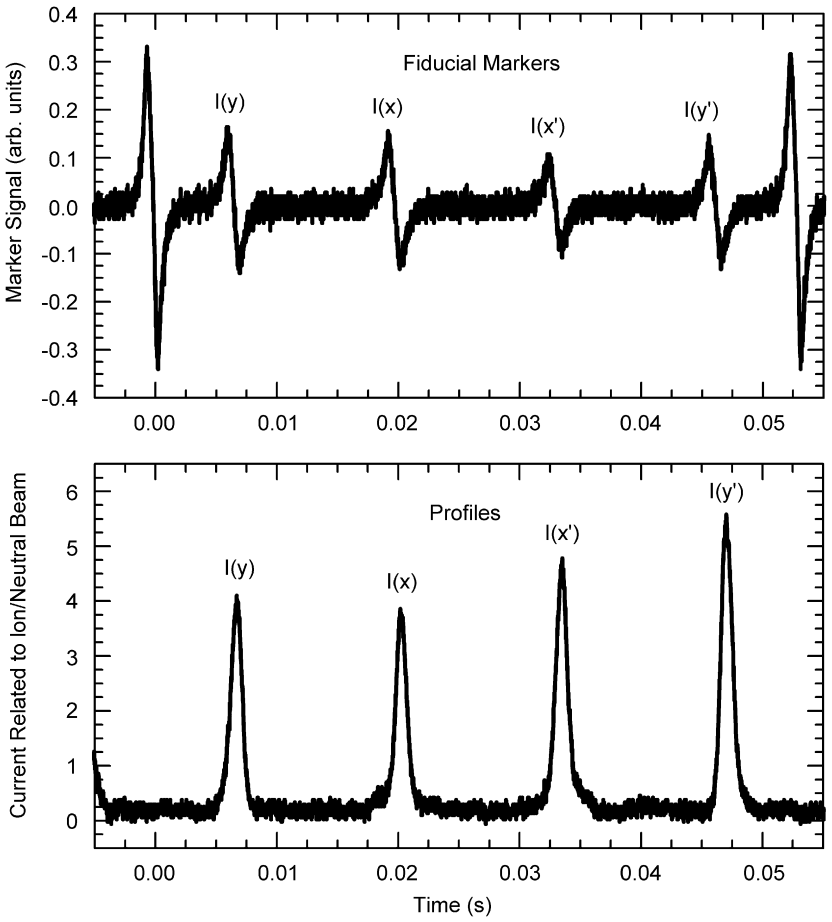

Fig. 3. The fiducial waveform (top) and profile waveform (bottom) from the scanner. The four smaller pulses that occur after the larger trigger pulse in the fiducial waveform identify the times when the wires pass through the centerline of the device creating the $I(y)$, $I(x)$, $I(x')$, and $I(y')$ profiles.

comprises $I_i(y)$, $I_i(x)$, $I_i(x')$, and $I_i(y')$ beam profiles, where x' and y' specify a coordinate system aligned with x and y, but located at a position z' that is further downstream along the beam axis by a distance determined by the geometry of the particular profile monitor that is used. The distance d between these locations is 5.4 cm for the BPM80 beam scanner [17]. In the waveform of fiducial pulses, the distance d corresponds to the time between the first and third fiducial pulses that occur after the trigger pulse.

A rotating wire scanner can measure profiles for each beam in a merged beams experiment if the profiles are acquired separately. In practice, this means that only one of the beams is admitted into the interaction region at a time, and the profiles of this beam are saved, e.g., as a waveform in a digital oscilloscope. Profiles of the second beam can then be acquired and displayed relative to the saved profiles of the first.

The dual wire scanner was installed on the ion-atom merged-beams apparatus at Oak Ridge National Laboratory [1], which is designed to measure low energy absolute charge transfer cross sections between ions and neutral atoms. In our studies of the response of this device, a 114 keV O^{5+} ion beam (typical current density of $1\,\mu A/mm^2$) was merged with a 9 keV neutral atomic hydrogen particle beam (typical equivalent current density of $10\,nA/mm^2$). The apparatus also has two sets of motor driven plates, each with two narrow non-overlapping orthogonal slits [6]. The slits in these assemblies make angles of 45° with the horizontal and vertical directions and allow a fraction of the beam to be transmitted to a Faraday cup located downstream. The slit assemblies are located before and after the dual wire scanner and generate beam profiles at 45° relative to the horizontal and vertical directions. These profiles can be used to check for irregularities in the beam profiles. The slit assemblies move much more slowly than the rotating wire scanner and intercept the beam, so they are not useful during tuning.

During the course of these investigations, the hydrogen beam was very stable in time; its beam profiles did not change measurably over periods exceeding several hours. Profiles of this beam were nonetheless saved and checked approximately every 15–30 min. Profiles of the ion beam were acquired during tuning and compared to the neutral beam profiles and the overlap functions $\Omega(z)$ and $\Omega(z')$ were then computed in real time. As is the case in all of our investigations, ion and neutral beams are accelerated to keV energies and are merged over a distance of 32.5 cm. To minimize the energy uncertainty, we typically limit the angular divergences of the beams to values less than about 0.35° to investigate collisions with energies between 0.01 and 1.0 eV/amu in the center of mass frame [1].

3. Real-time analysis

The preamplified signal and fiducial outputs of the modified scanner were connected to a Tektronix DPO4034 four-input digital phosphor oscilloscope which was interfaced to a laboratory computer via LabVIEW. The DPO4034 has extensive waveform inspection and save features and a user-selectable record length, settable in decades, which specifies the number of memory locations (or channels) that will be allocated to each oscilloscope trace. We chose a record length for each scan of 10^4 channels and a time span of 100 ms for each trace. The scanner rotates at a rate of about 18.9 revolutions/s, so the waveform associated with one rotation of the wire scanner requires about 5300 oscilloscope channels. As noted previously, the scanner was calibrated by the manufacturer so that the time interval between the zero crossings of the first and third fiducial pulses that occur after the trigger pulse can be used for an accurate determination of the beam profiles in the immediate vicinity of the fiducial marks. For the NEC BPM80 model used here, the calibration distance resulting from the scanning diameter

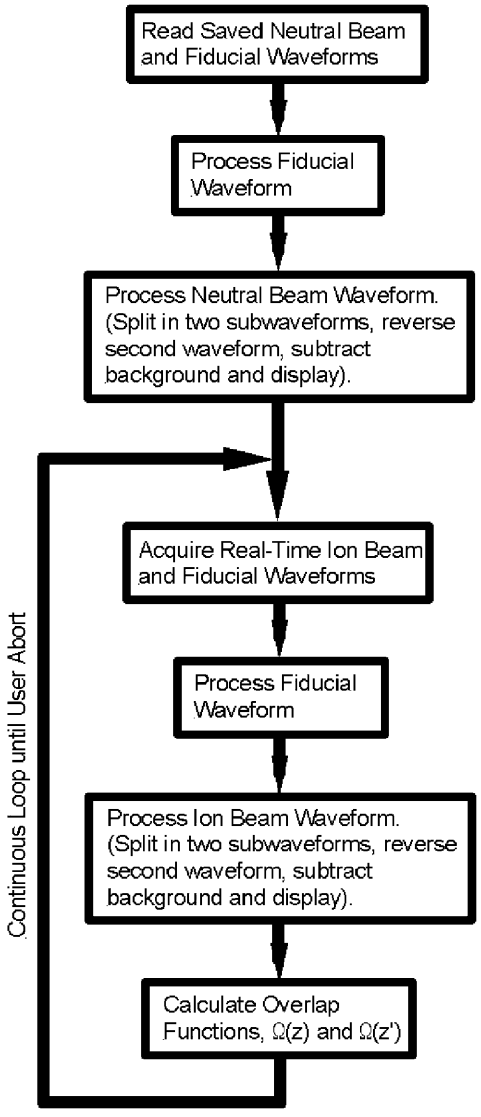

Fig. 4. Schematic overview of LabVIEW code. It is assumed that when the code is invoked, the signal waveform associated with one of the beams and its fiducial waveform have already been acquired and saved in the oscilloscope and that the profile monitor is scanning the second beam.

of 5.4 cm is 6.0 cm [17]. The zero crossings were separated by 2647 ± 2 oscilloscope channels from which we infer that a distance of 1.00 cm in the x or y directions in each pseudoplane corresponds to about 441 channels in the vicinity of the fiducial marks. Thus, each channel corresponds to a distance of about 0.023 mm. The diameter of the scanning wire is 0.5 mm, which corresponds to about 22 channels with these settings. In practice, the resolution of the system is on the order of 1 mm because of the thickness of the wire, which tends to introduce a slight broadening in the measured profile. Numerical simulations indicate that the measured profile of a Gaussian beam with a full width at half maximum (FWHM) of 1.5 mm (typical for our experiments) will have a FWHM that is between two and three percent larger than the actual value.

An overview of the LabVIEW code used to read out the oscilloscope and to extract the beam profile and beam–beam overlap information is shown in Fig. 4. Before the code is invoked, the signal waveform associated with the first beam (in our case, the neutral beam) and its fiducial waveform must have been acquired and saved in the oscilloscope. It also assumes that the second beam (in our case, the ion beam) has been admitted into the merge section and is currently being scanned. The LabVIEW code first reads the current configuration settings of the oscilloscope and adjusts the time setting, if necessary, to be the value listed above. It then reads the saved beam profile and fiducial waveforms, which in our case were the saved profile and fiducial waveforms of the neutral beam. The fiducial waveform is processed first. The code identifies the locations of the five fiducial pulses in the waveform. After the trigger pulse is identified, the instants when the wires cross the centerline of the scanner are identified by second order polynomial fits to the zero crossings of the remaining four fiducial pulses. Channel numbers are then converted to distance and displayed on the computer screen showing the beam profiles.

The saved beam profile waveform is processed next. Only that part of the waveform that occurs between the fiducial waveform trigger pulses is saved. This waveform is split in half, so that the first subwaveform contains $I_1(y)$ and $I_1(x)$ beam profiles, while the second subwaveform contains $I_1(x')$ and $I_1(y')$ beam profile waveforms. The second subwaveform is then reversed so that the directions of transit of the wires correspond to the directions traversed in the first subwaveform. The small background ("DC") component of each subwaveform is then determined and subtracted, each subwaveform is separately normalized to its peak value, and the results are displayed in two vertically stacked plots. In this way, the beam divergence in either x or y directions is easy to see in a qualitative way.

The profile and fiducial waveforms of the second beam (in our case, the ion beam) are acquired in real time. The fiducial and beam profile waveforms are processed in the same manner as the saved waveform (i.e. the first subwaveform contains $I_2(y)$ and $I_2(x)$ beam profiles, while the second subwaveform contains $I_2(x')$ and $I_2(y')$ beam profile waveforms). The plots are updated as fast as the data can be transferred and processed, which is about four acquisitions per second in our application, or roughly every

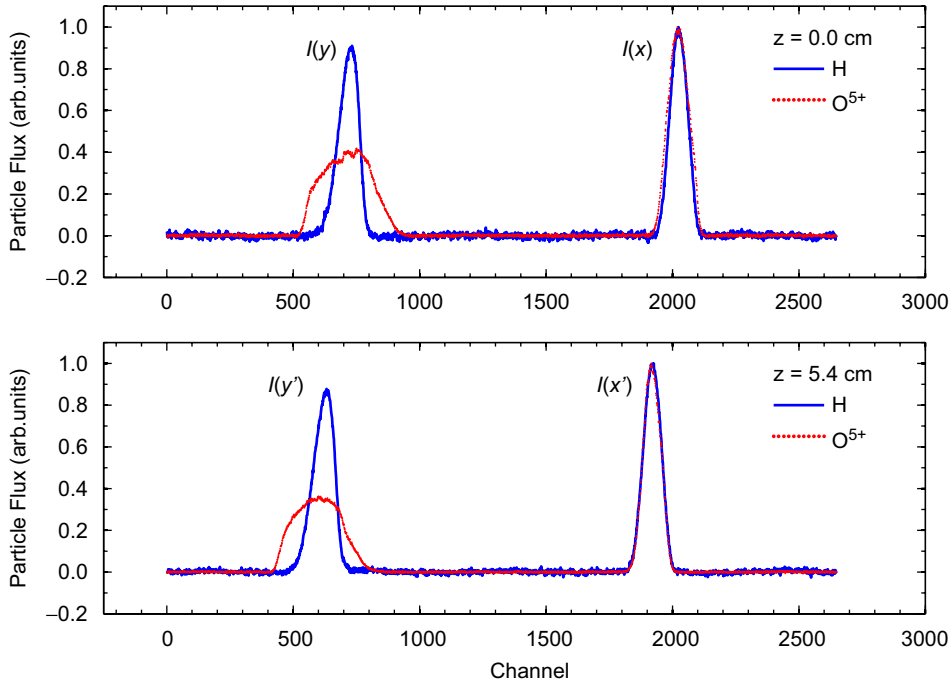

Fig. 5. The processed waveforms from the LabVIEW program for a 114 keV O^{5+} beam and 9.00 keV H beam. The upper part shows the vertical (y) and horizontal (x) profiles in the first (upstream) pseudoplane. The lower part shows the corresponding profiles in the second (downstream) pseudoplane. Note in each pseudoplane the near perfect overlap in the horizontal profiles. The beam–beam overlap given by Eq. (6) improved slightly between $z = 0$ and 5.4 cm, from 5.65 to 6.58 cm^{-2}.

Table 1
Full width at half maximum (FWHM) distances and angular divergence (half angle) of each of the profiles shown in Fig. 5

	H beam		O^{5+} beam	
	Vertical	Horizontal	Vertical	Horizontal
FWHM ($z = 0.0$ cm)	2.0 mm	1.8 mm	5.4 mm	2.2 mm
FWHM ($z = 5.4$ cm)	2.1 mm	1.8 mm	5.0 mm	1.8 mm
Angular divergence (half angle)	0.05°	$<0.024°$	0.21°	0.21°
	Diverging	Parallel	Converging	Converging

fifth scan of the wire across the beam. This processing rate is sufficiently fast for beam tuning. Profile waveforms that are acquired by the oscilloscope while the LabVIEW code is processing a waveform are not used. Each time the LabVIEW display is updated, the beam overlap functions, $\Omega(z)$ and $\Omega(z')$ are calculated and displayed.

Sample output from the LabVIEW application for 114 keV O^{5+} ions merged with 9.00 keV H-atoms is shown in Fig. 5. The normalized $I_2(y)$ and $I_2(x)$ beam profiles are displayed on the same plot that contains the $I_1(y)$ and $I_1(x)$ beam profiles, while the reversed $I_2(x')$ and $I_2(y')$ are displayed on their corresponding plot. Clearly, these beams are well merged in both the horizontal (x) and vertical (y) directions, and the degree to which the beams overlap in the vertical direction is very high. It is also evident that the width of ion beam in the horizontal direction is approximately twice that of the neutral beam. It is possible to determine and compare the relative particle fluxes from the measured profiles before the normalization if one so desires.

Each of the profiles shown in Fig. 5 are also fitted by a Gaussian function to estimate the angular divergence of each beam between the two pseudoplanes. The FWHM values are used to determine the angular divergence of each beam. The results of this analysis are shown in Table 1. The beam–beam overlap integral given by Eq. (6) improved slightly between $z = 0$ and 5.4 cm, from 5.65 to 6.58 cm^{-2}.

4. Summary

The rotating dual wire beam scanner (modified from a NEC BPM80 beam scanner) in conjunction with the Tektronic DPO4034 digital oscilloscope and LabVIEW software has proven to be a useful compact beam profile monitoring system which provides accurate horizontal and vertical profiles at two locations along the beam axis. This device is especially useful in the extensive beam tuning required in a merged-beams experiment where the merge angle between beams and the divergence of each beam must be minimized and the beam–beam overlap maximized and displayed in real time.

Acknowledgements

This research is supported by the DOE, Division of Chemical Sciences, Office of Basic Energy Sciences and the Division of Applied Plasma Physics, Office of Fusion Energy Sciences, under Contract no. DE-AC05-00OR22725. DGS gratefully acknowledges support from the Great Lakes Colleges Association Oak Ridge Science Semester program and Albion College. HB and DWS were supported in part by NSF Stellar Astronomy and Astrophysics Grant no. AST-0606960 and NSF Chemistry Instrument Development Grant no. CHE-0520660.

References

[1] C.C. Havener, in: F.J. Currell (Ed.), The Physics of Multiply and Highly Charged Ions, Kluwer Academic Publishers, Dordrecht, 2003, p. 193.
[2] R.A. Phaneuf, C.C. Havener, G.H. Dunn, A. Muller, Rep. Prog. Phys. 62 (1999) 1143.
[3] D. Auerbach, R. Cacak, R. Caudano, T.D. Gaily, C.J. Keyser, J.Wm. McGowan, J.B.A. Mitchell, S.F.J. Wilk, J. Phys. B 10 (1977) 3797.
[4] C.J. Keyser, H.R. Froelich, J.B.A. Mitchell, J.W. McGowan, J. Phys. E 12 (1979) 316.
[5] K. Olamba, S. Szücks, J.P. Chenu, N. El Arbi, F. Brouillard, J. Phys. B 29 (1996) 2837.
[6] C.C. Havener, in: S.M. Shafroth, J.C. Austin (Eds.), Applications-Based Atomic Physics Techniques and Applications, AIP, New York, 1997, p. 117.
[7] D.E. Nitz, M.W. Geis, K.A. Smith, R.D. Rundel, Rev. Sci. Instr. 47 (1976) 306.
[8] J.L. Forand, C. Timmer, E. Wahlin, B.D. DePaola, G.H. Dunn, D.R. Swenson, K. Rinn, Rev. Sci. Instr. 61 (1990) 3372.
[9] S.K. Sethuraman, J.R. Gibson, J.L. Moruizzi, J. Phys. E 10 (1977) 14.
[10] G. Hortig, Nucl. Instr. and Meth. 30 (1964) 355.
[11] J.W. Jagger, J.G. Page, P.J. Riley, Nucl. Instr. and Meth. 49 (1967) 121.
[12] C.D. Bond, S.E. Gordon, Nucl. Instr. and Meth. 98 (1972) 513.
[13] C.C. Havener, R. Al-Rejoub, United States Patent 6972551, UT-Batelle, LLC, Oak Ridge, TN.
[14] National Electrostatics Corporation, Middleton, WI 53562-0310.
[15] National Electrostatics Corporation Instruction Manual for Model BPM80 Beam Profile Monitor.
[16] National Electrostatics Corporation current amplifier, Model 2HA003090, provided with the BPM80 Beam Profile Monitor system.
[17] The distance that either of the wires moves during a half rotation (corresponding to the time between the first and third fiducial pulses) is πr, where r is the radius of the scanning circle. Because the device is tilted 45° relative to the xy coordinate frame, this distance projected onto either the x or y axis is $\pi r/\sqrt{2}$. For the BPM80 scanner, the scanning circle radius $r = 2.7$ cm, which gives a calibration distance of 6.0 cm between the first and third fiducial positions.